AGU100 ADVANCING EARTH AND SPACE SCIENCE

Geophysical Research Letters

RESEARCH LETTER

10.1029/2018GL078482

Key Points:
- Signatures of a magnetic dip were observed in the near-Earth plasma sheet
- Interchange heads in the dip drifted toward dawn
- Switching to dawnward drifting is due to current sheet charging

Supporting Information:
- Text S1
- Text S2
- Data Set S1
- Data Set S2
- Data Set S3
- Data Set S4

Correspondence to:
E. V. Panov,
Evgeny.Panov@oeaw.ac.at

Citation:
Panov, E. V., & Pritchett, P. L. (2018). Dawnward drifting interchange heads in the Earth's magnetotail. *Geophysical Research Letters*, *45*, 8834–8843. https://doi.org/10.1029/2018GL078482

Received 23 APR 2018
Accepted 27 AUG 2018
Accepted article online 4 SEP 2018
Published online 14 SEP 2018

Dawnward Drifting Interchange Heads in the Earth's Magnetotail

E. V. Panov[1] **and P. L. Pritchett**[2]

[1]Space Research Institute, Austrian Academy of Sciences, Graz, Austria, [2]Department of Physics and Astronomy, University of California, Los Angeles, CA, USA

Abstract A fortuitous configuration of five Time History of Events and Macroscale Interactions during Substorms probes indicated that on 15 February 2008 between 04:00 and 11:00 UT a B_Z dip with radial size of about 2.5 Earth radii (R_E) and azimuthal size that could be as large as 10 R_E was present for over 3 hr in the plasma sheet at $X_{GSM} \approx -11$ R_E. Ballooning/InterChange Instability heads were observed at the tailward side of the dip with $\partial B_Z/\partial X \approx -10$ nT/R_E. The Ballooning/InterChange Instability heads appeared to drift azimuthally toward dawn, in accord with particle-in-cell simulations of a charged current sheet. The signatures of the latter, for example, a finite average E_Z directed toward the center of the plasma sheet, are verified by the Time History of Events and Macroscale Interactions during Substorms data.

Plain Language Summary On the antisunward side of the Earth, the terrestrial magnetic field lines are stretched out to form an elongated structure called the magnetotail. At the center of this structure the magnetic field strength normally decreases continually with increasing distance away from the Earth. However, periodically, the magnetotail is disrupted in a process called a substorm; the cause of this disruption remains controversial. A fortuitous configuration of five space probes is used to investigate a possible mechanism for this disruption. The probes observed the formation of a substantial region where the magnetic field strength possessed a minimum (rather than always decreasing). By comparing with the results of plasma computer simulations, it is shown that this region should generate an instability that produces dawnward propagating clumps of more dipolar field lines, in agreement with the probe observations.

1. Introduction

The interface between the dipole and stretched field lines of the Earth's magnetotail around $X_{GSM} \approx -11$ R_E can be the site of a magnetic field minimum (e.g., Saito et al., 2010). The minimum may be formed, for example, as a feature of global steady convection in ideal magnetohydrodynamic models (Hau, 1991; Hau et al., 1989), or when simultaneous adiabatic lobe compression and sunward convection remove closed magnetic flux in the near-Earth tail (Hsieh & Otto, 2015). Another mechanism for forming the magnetic field minimum would be to create a diamagnetic thin current sheet in the transition region between the dipole and tail fields (Pritchett & Coroniti, 1994, 1995). The imposition of a dawn to dusk electric field E_y in the transition region would lead to charge-separation effects as a result of a slow earthward convection of plasma and a large tailward transfer of magnetic flux. One consequence of the charge-separation effects is a finite average E_Z directed toward the center of the plasma sheet that serves to confine the ions electrostatically.

Magnetotail configurations with a magnetic field minimum contain a tailward gradient of B_Z and may be unstable to a kinetic Ballooning/InterChange Instability (BICI; Pritchett & Coroniti, 2010; Sitnov et al., 2014). BICI would generate azimuthally thin earthward intrusions (heads) of depleted plasma tubes; the strongest of these are expected to provoke reconnection onset (Pritchett & Coroniti, 2011, 2013). Recent Time History of Events and Macroscale Interactions during Substorms (THEMIS) observations showed that the BICI may be responsible for generation of sausage-type magnetic oscillations that propagate across the near-Earth plasma sheet in the duskward direction (Panov, Nakamura, et al., 2012; Panov, Sergeev, et al., 2012). The oscillations are associated with the characteristic field-aligned electron flows and may be followed by a substorm onset.

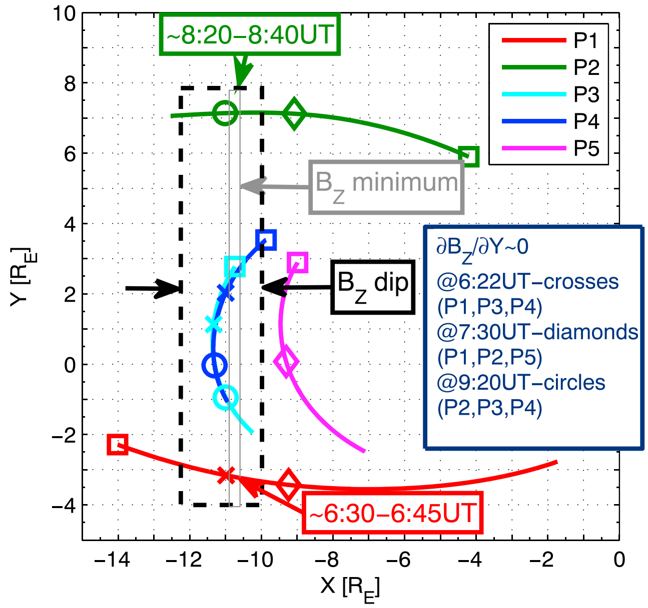

Figure 1. Orbit segments for Time History of Events and Macroscale Interactions during Substorms probes P1 (red), P2 (green), P3 (cyan), P4 (blue), and P5 (magenta) on 15 February 2008 between 04:00 and 11:00 UT in *XY* geocentric solar magnetospheric plane. Probe's positions are denoted by squares at 4:00 UT, by crosses at 6:22 UT, by diamonds at 7:30 UT, and by circles at 9:20 UT.

Independent auroral observations around the breakup initiation exhibit various auroral structures like azimuthally spaced auroral forms (AAFs) with mode numbers between few tens and more than one hundred (Elphinstone et al., 1995) and also beads and rays (Donovan et al., 2006; Gallardo-Lacourt et al., 2014; Kalmoni et al., 2015; Liang et al., 2008; Motoba, Hosokawa, Kadokura, & Sato, 2012; Motoba, Hosokawa, Ogawa, et al., 2012; Nishimura et al., 2014, 2016; Rae et al., 2010; Sakaguchi et al., 2009; Tang, 2011; Uritsky et al., 2009). These studies have suggested that AAFs and beads/rays are ionospheric manifestation of a ballooning-type mode operating in the near-Earth plasma sheet. The auroral observations, however, have shown that auroral onset beads/rays can propagate dawnward as well as duskward, with the dawnward direction actually being more common. Nishimura et al. (2016) showed that the BICI mechanism for generating such onset beads can also account for the dawnward propagation cases if one extends the model to the case of charged current sheets where the electrons carry the cross-tail current.

In the present investigation we use magnetotail observations provided by the THEMIS (Angelopoulos, 2008) probes' fluxgate magnetometers (Auster et al., 2008), electrostatic analyzers' (McFadden et al., 2008) particle detectors and electric field instruments (Bonnell et al., 2008) on 15 February 2008 to show evidence of the presence of a B_Z dip with radial size of about 2.5 R_E and azimuthal size that could be as large as 10 R_E for over 3 hr in the plasma sheet at $X_{GSM} \approx -11$ R_E. Further, we employ the particle-in-cell (PIC) simulation run from Nishimura et al. (2016) of the BICI development in a charged current sheet to show that the intense magnetic oscillations observed by THEMIS at the tailward side of the B_Z dip with $\partial B_Z/\partial X \approx -10$ nT/R_E, which propagate dawnward at a velocity of about 0.3 times the ion thermal velocity and exhibit a characteristic finite average E_Z directed toward the center of the plasma sheet, can be identified as magnetotail BICI heads.

2. Global Plasma Sheet Development

Figure 1 shows orbit segments for THEMIS probes P1 (red), P2 (green), P3 (cyan), P4 (blue), and P5 (magenta) on 15 February 2008 between 04:00 and 11:00 UT in *XY* geocentric solar magnetospheric (GSM) plane. During this time interval, the three probes P3–P5 were crossing the magnetotail mainly azimuthally from dusk to dawn at X_{GSM} between −11 and −7 R_E. In contrast, P2 was located duskward from P3 to P5 and was moving tailward from $X_{GSM} \approx -4.3$ R_E to $X_{GSM} \approx -12.5$ R_E, and P1 was located dawnward from P3 to P5 and was moving earthward from $X_{GSM} \approx -14$ R_E to $X_{GSM} \approx -1.8$ R_E. Hence, the THEMIS orbits permit the study of the transition region between the dipole and tail fields in 2-D, both azimuthally and radially.

Figures 2a and 2b show the B_X and B_Z magnetic field components, and Figures 2c and 2d show the *X* and *Y* GSM coordinates for P1–P5 on 15 February 2008 between 4:00 and 11:00 UT. P1 was crossing the X_{GSM} location of P3–P5 between about 6:10 and 7:30 UT. P2 was crossing the X_{GSM} location of P3–P5 between about 7:30 and 9:30 UT. Probes P1 and P2 appeared to cross the same X_{GSM} at about 7:30 UT. During these three occasions, probes P1, P3, and P4 around 6:22 UT, probes P1, P2, and P5 around 7:30 UT and probes P2, P3, and P4 around 9:20 UT were located at similar X_{GSM} (denoted by dark blue rectangles in Figure 2c). As Figure 2b indicates, the corresponding probes measured similar B_Z around the three times (the traces of B_Z in Figure 2b cross each other; highlighted by the three dark blue arrows that originate from the three rectangles). This fact suggests that the azimuthal gradient of B_Z ($\partial B_Z/\partial Y$) was small (1) between P1 and P4 ($X_{GSM} \approx -11R_E$; -3 $R_E < Y_{GSM} < 2$ R_E) around 6:22 UT, (2) between P1 and P2 ($X_{GSM} \approx -9.2R_E$; -3.5 $R_E < Y_{GSM} < 7.2$ R_E) around 7:30 UT, and (3) between P4 and P2 ($X_{GSM} \approx -11R_E$; -1 $R_E < Y_{GSM} < 7.2$ R_E) around 9:20 UT (positions of the corresponding THEMIS probes during the three occasions are indicated by crosses, diamonds and circles in Figure 1). Additionally, P3 and P4 were located at nearly identical X_{GSM} between about 6:35 and 9:10 UT and detected similar B_Z values. Hence, during this time $\partial B_Z/\partial Y$ at -1 $R_E < Y_{GSM} < 2$ R_E was permanently small too (highlighted by a thick horizontal blue bar under Figure 2d). The above conclusions on $\partial B_Z/\partial Y$ suggest that the plasma sheet had approximately a 1-D current sheet between 6:20 and 9:30 UT. Hence, during this time interval one can estimate $\partial B_Z/\partial X$ from

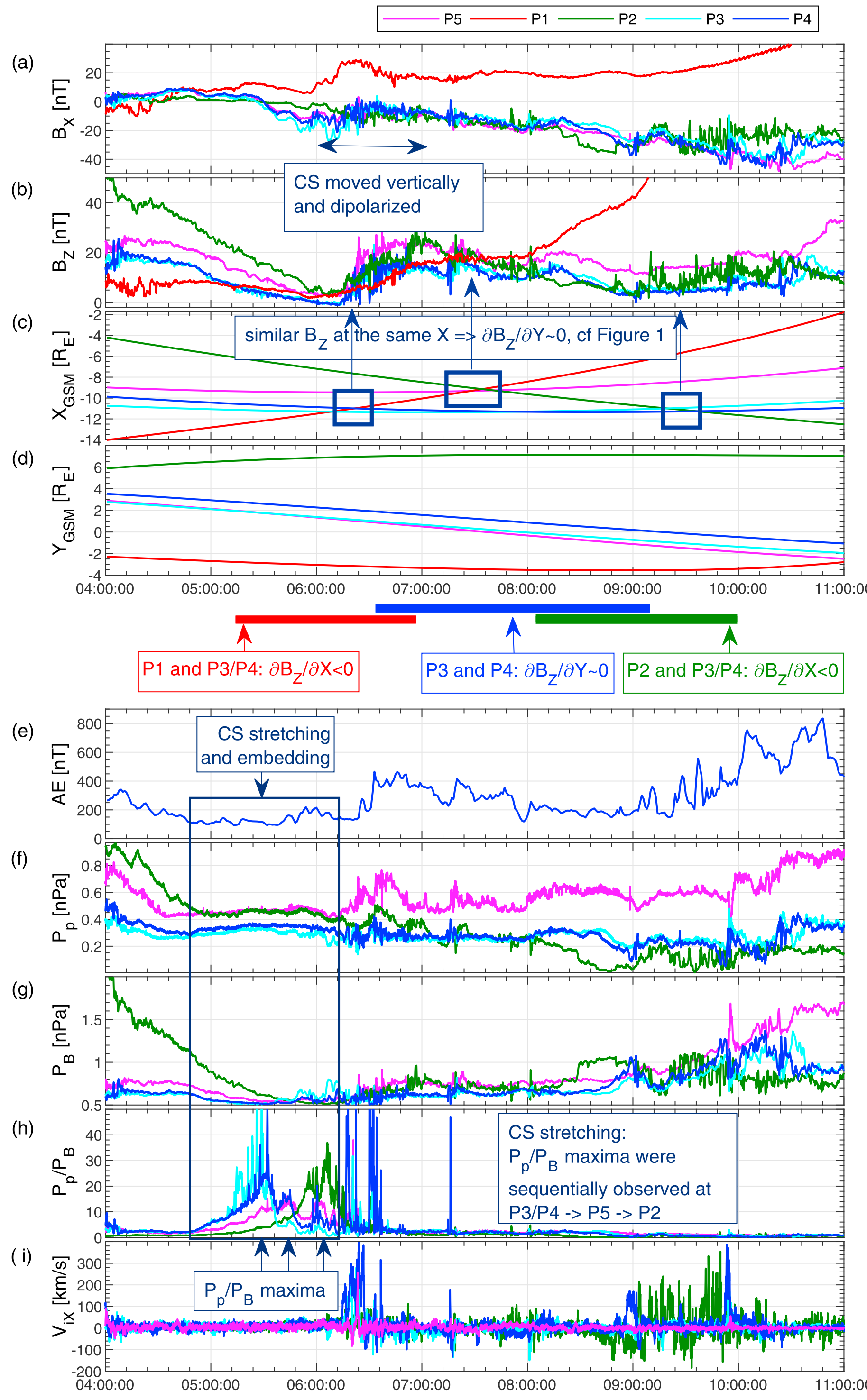

Figure 2. Five Time History of Events and Macroscale Interactions during Substorms probes' observations on 15 February 2008 between 4:00 and 11:00 UT: (from top to bottom) B_X (a) and B_Z (b) geocentric solar magnetospheric (GSM) magnetic field components, X (c) and Y (d) GSM coordinates, AE index (e), plasma pressure (f), magnetic pressure (g), plasma beta (h), and the V_X GSM ion velocity component. The color coding is the same as in Figure 1.

probe pairs that were located at the same distance to the current sheet center but were separated along the Y_{GSM} axis. Note that between about 6:00 and 6:18 UT the plasma sheet moved southward and after 6:18 UT northward as it is seen from B_X in Figure 2a and confirmed by the ion velocity V_Z at P2–P5 of about few tens of kilometers per second (not shown). The southward plasma sheet motion made P1 be located farther from the current sheet center than P2–P4 and imply some ambiguity between $\partial B_Z/\partial X$ and $\partial B_Z/\partial Z$. Also, at 6:15 UT a plasma sheet dipolarization was observed by all probes as can be seen from B_Z in Figure 2b, which also significantly affected the values of B_Z and potentially $\partial B_Z/\partial X$.

Thus, before about 5:15 UT $\partial B_Z/\partial X$ was positive at X_{GSM} between −13 and −6 R_E. Between about 5:15 and 6:15 UT P1, being still more tailward than P3/P4, observed larger values of B_Z than P3/P4. This indicates $\partial B_Z/\partial X < 0$ at the tailward side of a local magnetic field minimum. P1 observed smaller values of B_Z than P3/P4 between about 6:20 and 7:00 UT when P1 appeared to be at X_{GSM} between P5 and P3/P4, that is, $\partial B_Z/\partial X < 0$, too. The two regions of $\partial B_Z/\partial X < 0$ are highlighted by a thick horizontal red bar under Figure 2d. P2 (green curves in Figure 2), which was moving tailward through the same X range as P1 but duskward from P3 to P5 observed a similar magnetic field behavior with $\partial B_Z/\partial X < 0$ between about 8:10 and 8:45 UT and between about 9:16 and 10:22 UT (highlighted by a thick horizontal green bar under Figure 2d). The area of the B_Z dip encountered by P1/P2 is schematically shown by the black dashed rectangle in Figure 1. Its radial extension encompasses about 2.5 R_E (at $-12.5\ R_E < X_{GSM} < -10\ R_E$). The times that correspond to the crossing of the B_Z minimum (grey rectangle in Figure 1) in the B_Z dip are indicated by the red (for P1) and the green (P2) text arrows.

Figures 2f–2h show the sum of the ion and electron pressures P_p, the magnetic pressure P_B, and the ratio of P_p to the magnetic field pressure P_B (plasma beta) from P1 to P5 during the interval. Slightly prior to and during the B_Z dip formation (between about 4:30 and 6:15 UT) the plasma pressure was observed to be stable at P2–P5 (Figure 2f; the electrostatic analyzer instrument at P1 did not downlink plasma data during the whole time interval). At the same time the magnetic pressure P_B (Figure 2g) decreased due to dropping of B_Z. This led to the growth of the plasma beta at the locations of P2–P5 from 1–2 up to 50. Hence, a thinner (embedded) current sheet within a thicker plasma sheet was forming during this time. Note that the embedded current sheet formation occurred first at P3/P4 between 4:45 and 5:30 UT, then at P5 between 5:00 and 5:45 UT, and finally at P2 between 5:10 and 6:10 UT. Hence, a radial (earthward) and azimuthal (duskward) stretching of the embedded current sheet was also observed. After 5:15 UT $|B_X|$ grew both in the Northern Hemisphere (at P1) and in the Southern Hemisphere (at P2–P5), indicating a further intensification of the embedded current sheet at all probes till about 6:15 UT (seen as decreases of plasma beta in Figure 2h just before 6:15 UT). Such intensification ended by a dipolarization at all probes (seen as growth of B_Z in Figure 2b after 6:15 UT) and by a structured moderate earthward flow (about 200 km/s on average) detected mainly at P4 (Figure 2i). These are associated with a sharp increase in the AE index around 6:30 UT from about 150 to about 400 nT (Figure 2e).

3. BICI Signatures and Propagation

The tailward side of the shown B_Z dip, which has emerged in the transition region between the dipole and tail fields ($X_{GSM} \approx -11\ R_E$) and persisted there for a few hours, is expected to be BICI unstable due to $\partial B_Z/\partial X < 0$. On the other hand, the observed formation of a thin current sheet between 4:30 and 6:00 UT suggests that a spatial rearrangement of the magnetic flux is supposed to have occurred during this time. At 5:15 UT P1 (the most tailward located probe) started to observe B_Z values larger than those at P3/P4 (more earthward located probes) due to slower B_Z reduction rate at P1 than at P3/P4. This fact indicates that the magnetic flux has indeed moved tailward from P3/P4 reaching out past P1. In this case the forming thin current sheet is expected to be charged, containing the E_Z directed toward the center of the plasma sheet.

Figure 3 shows the results from 3-D PIC simulation using the electron (charged) current sheet. This produces the dawnward propagating BICI heads as opposed to the previous cases in Pritchett and Coroniti (2010, 2013) and Pritchett et al. (2014), which considered only duskward propagating BICI heads. The boundary conditions in the present simulation are the same as those in Pritchett et al. (2014). In particular, the earthward boundary uses a *closed* condition in which no magnetic flux is allowed to cross the boundary. The simulation spatial coordinates are given in units of the ion gyroradius ρ_{i0} defined using the asymptotic (lobe) field B_0. Note that in this simulation the y coordinate is directed toward dawn, so that dawnward is toward increasing values of y. Figure 3a shows the early-stage ($\Omega_{i0}t = 169$) development of the BICI in the equatorial plane with the emergence of two longer-wavelength structures, while Figure 3c shows a stack plot for $168.7 \le \Omega_{i0}t \le 187.5$

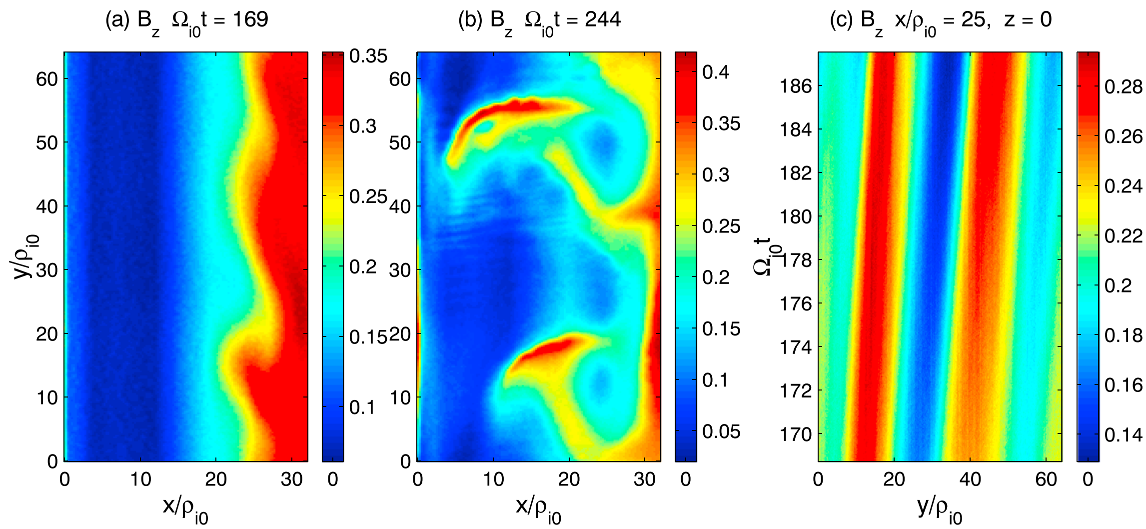

Figure 3. Results from 3-D particle-in-cell simulation using the electron (charged) current sheet. The *y* coordinate is directed toward dawn. (a, b) The early-stage ($\Omega_{i0}t = 169$) and later-stage ($\Omega_{i0}t = 244$) development of the Ballooning/InterChange Instability in the equatorial plane with the emergence of two Ballooning/InterChange Instability heads in each panel. (c) A stack plot for $168.7 \leq \Omega_{i0}t \leq 187.5$ at $x/\rho_{i0} = 25$.

at $x/\rho_{i0} = 25$, which makes clear the dawnward propagation. The propagation speed is about 0.35 times the ion thermal velocity. Figure 3b shows the late-time ($\Omega_{i0}t = 244$) development of the BICI in the equatorial plane that features two elongated heads that are thin in *y* but spread out in *x*.

The main difference in the charged current sheet equilibrium is that the ions are now at rest and the electrons carry the current. Figure 4 shows the properties of a single BICI head as reflected in various electric field components for the present charged current sheet. The results are plotted in a y, z plane at $x/\rho_{i0} = 6$ at time $\Omega_{i0}t = 244$. Note that the off-axis oscillations in the head are the ion cyclotron oscillations, which are quite similar to those in the earlier simulations of a neutral current sheet (Pritchett et al., 2014; not shown here) with oscillation amplitude $cE_y/V_{Ti}B_0 \sim 2$ and a similar wavelength (Figure 4a). Figure 4b shows the E_z component. In contrast to the neutral sheet case, in the charged sheet, there is a clear bipolar (Hall) field directed toward the center of the sheet with peak magnitude $cE_z/V_{Ti}B_0 \sim 1.5$. This Hall field is modulated by the ion cyclotron waves but does not change sign. In the neutral sheet, there are similar off-axis oscillating fields with a similar magnitude, but these fields are shielded at smaller $|z|$ by an opposite-sign oscillating field. Figure 4c shows the parallel field $E_{||}$. This field is much weaker (by a factor of 20 for the charged sheet) and is confined close to the equatorial plane at $|z/\rho_{i0}| < 1$. At the location of the strong wave fields, the $E_{||}$ fields are 5% or less of the wave fields. This latter fact allows us to compare with THEMIS observations using the E_Z component of the electric field that is computed from E_X and E_Y assuming that $(E \cdot B) = 0$.

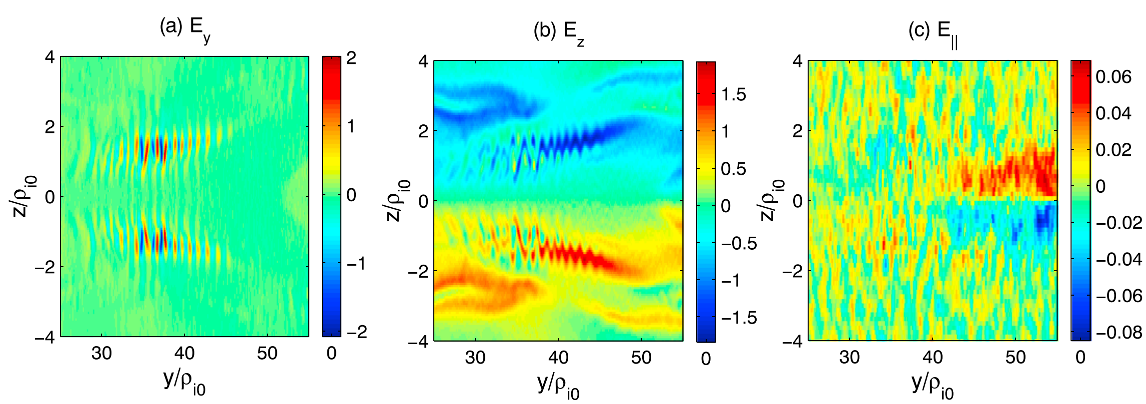

Figure 4. Properties of one Ballooning/InterChange Instability head as reflected in E_y (a), E_z (b), and $E_{||}$ (c) electric field components for the present charged current sheet. The results are plotted in a y, z plane cut at at $x/\rho_{i0} = 6$ at time $\Omega_{i0}t = 244$.

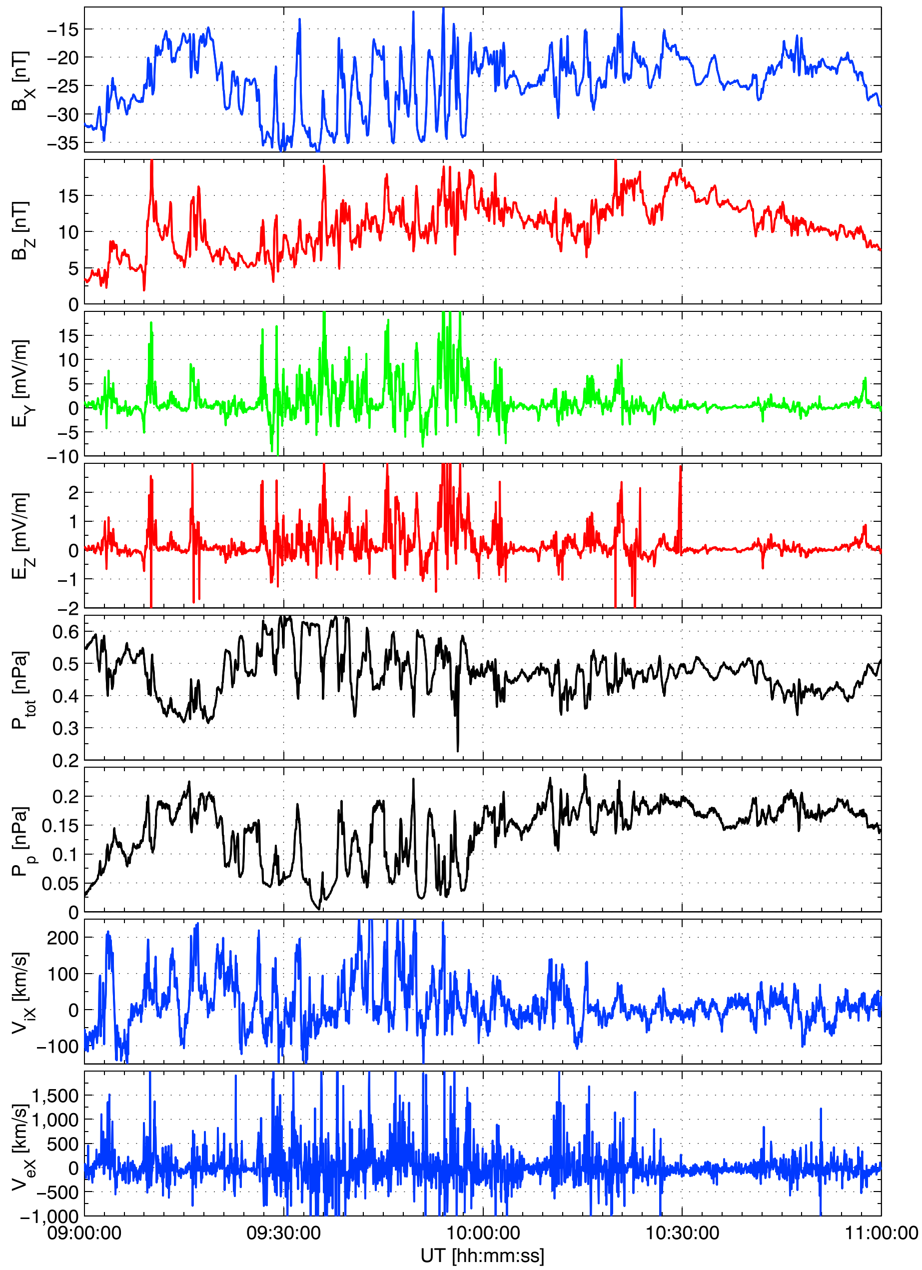

Figure 5. Time History of Events and Macroscale Interactions during Substorms probe P2 observations on 15 February 2008 between 9:00 and 11:00 UT: (from top to bottom) B_X, B_Z magnetic and E_Y, E_Z electric field geocentric solar magnetospheric components (E_Z was calculated from E_X and E_Y assuming $(E \cdot B) = 0$.), total (sum of the magnetic, ion, and electron) and particle (sum of the ion and electron) pressures, ion, and electron X DSL velocity components.

On 15 February 2008 between 09:00 and 11:00 UT THEMIS probes P2, P3, and P4 were at about $X_{GSM} \approx -11\ R_E$ downtail. They were separated mainly in the Y_{GSM} direction, with the most duskward P2 located near $Y_{GSM} = 7R_E$ and the most dawnward P3 around $Y_{GSM} = -1.3R_E$. P4 was located about 1 R_E duskward and for the most of time slightly tailward from P3. Hence, such a spacecraft configuration is ideal for studying magnetotail structures that propagate in the azimuthal direction, for example, BICI heads.

Since BICI is a low-frequency generalization of the lower-hybrid drift instability to a curved magnetic field geometry (Pritchett & Coroniti, 2010), the dominant polarizations of the BICI and lower-hybrid drift instability modes coincide, being the electrostatic potential and the parallel magnetic field. Particularly expected

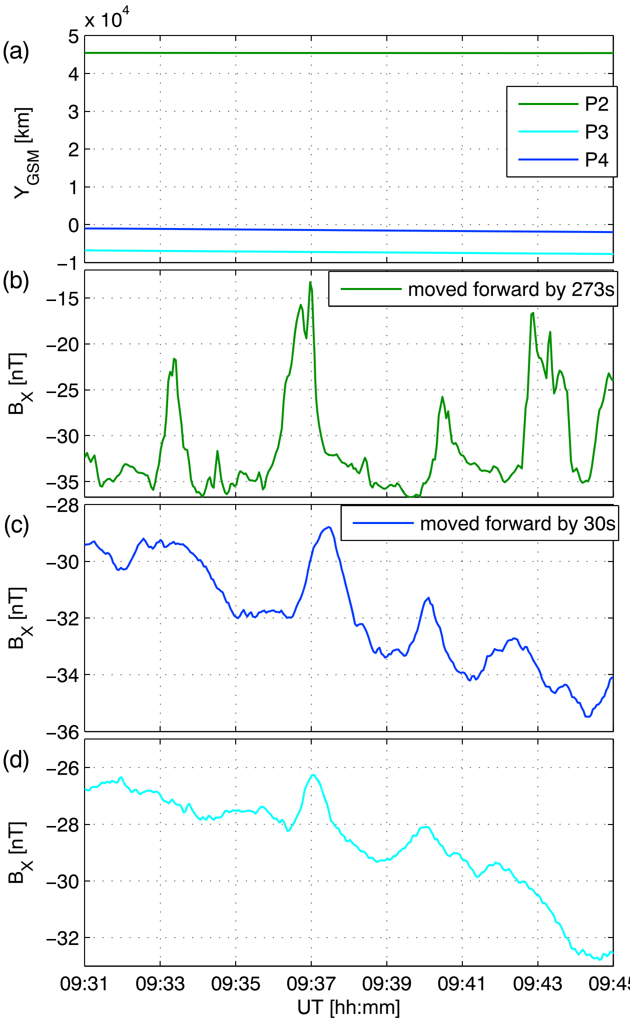

Figure 6. Time History of Events and Macroscale Interactions during Substorms probe P2, P3, and P4 observations on 15 February 2008 between 9:31 and 9:45 UT: Y_{GSM} coordinate of P2 (green), P3 (cyan), and P4 (blue) location (a), GSM B_X magnetic field component from P2 (b), P4 (c), and P3 (d). The P2 (P4) B_X is shifted by 273 s (30 s) forward.

are the correlations of the electron density (particle pressure) and the parallel magnetic field and of the electron parallel velocity with the perpendicular electric field. Thus, previous THEMIS (Panov, Nakamura, et al., 2012; Panov, Sergeev, et al., 2012) observations exhibited BICI signatures including strong magnetic oscillations with periods 20–100 s and δB_X about 10–20 nT. Associated with these were oscillations of the electric field δE_Y ~1 mV/m and the field-aligned electron velocity of several hundreds of kilometers per second. No comparable perturbations in the ion velocity were observed. The δB_X and δB_Z oscillations were in phase; the electric field E_Y oscillations were phase shifted by $\pi/2$.

Figure 5 shows THEMIS probe P2 observations on 15 February 2008 between 9:00 and 11:00 UT: (from top to bottom) B_X, B_Z magnetic and E_Y, E_Z electric field GSM components (E_Z was calculated from E_X and E_Y assuming $(E \cdot B) = 0$.), total (sum of the magnetic, ion, and electron) and particle (sum of the ion and electron) pressures, ion and electron X DSL velocity components (close to the antiparallel magnetic field direction). Hence, in agreement with previous BICI signature observations, these P2 observations (mainly between 9:30 and 10:00 UT) exhibit strong oscillations with periods about 150 s in δB_X up to 20 nT and stronger δE_Y sometimes exceeding 15 mV/m. As P2 moved tailward between 9:00 and 10:30 UT from about $X_{GSM} \sim -10.5\, R_E$ to $X_{GSM} \sim -12\, R_E$ the observed magnetotail B_Z grew from about 5 to over 15 nT, suggesting that P2 moved further away from a local B_Z minimum. After 10:30 UT B_Z at P2 decreased back to about 7 nT, simultaneously with decreasing of the oscillation amplitude in B_X. Note that E_Z was more positive than negative, that is, with a background value exceeding 0.5 mV/m and directed toward the center of the plasma sheet (P2 was located in the Southern Hemisphere during the whole time interval). The two further panels in Figure 5 show that although the plasma pressure was clearly anticorrelated with the magnetic pressure (seen from B_X), it could never compensate it. This fact would be in agreement with the idea that P2 observed intermittently flux tubes with different entropy values, that is, BICI heads. The two bottom panels in Figure 5 show that both ions and electrons exhibit parallel flows, which are strongly structured. Again, in agreement with BICI PIC simulations (Pritchett & Coroniti, 2010) and THEMIS observations (Panov, Nakamura, et al., 2012; Panov, Sergeev, et al., 2012), the parallel electron flows are much stronger than those of ions.

Figure 6 shows THEMIS probe P2, P3, and P4 observations on 15 February 2008 between 9:31 and 9:45 UT: Y_{GSM} coordinate of P2 (green), P3 (cyan), and P4 (blue) location (a), GSM B_X magnetic field component from P2 (b), P4 (c), and P3 (d). The P2 (P4) B_X is shifted by 273 s (30 s) forward. One can see that the four shown B_X dips at about 9:33:15, 9:37, 9:40, and 9:42:30 UT (correspond to four BICI heads) on average moved from P4 to P3 (i.e., about 5,800 km dawnward) within about 30 s. This implies a dawnward propagation velocity of about ≈193 km/s. Based on this velocity, the expected time delay between P2 and P3 would be about 273 s (Figure 6b). Taking into account the ion temperature of about 4–5 keV (not shown here), the propagation velocity is about 0.3 times the ion thermal velocity. Hence, the propagation velocity is close to the predictions of the PIC simulations in Figure 3.

4. Discussion

The four dips in B_X in Figure 6 do not exactly repeat themselves even at the closely located probes P3 and P4, whose azimuthal separation was about 1 R_E, that is, only about half-width of the BICI heads. The four dips at P3 and P4 are yet less similar to the four dips at P2, which was 9 times farther away from P4 than P3. Such staggering in the dips observation at different probes is expected because (1) the BICI heads may evolve from probe to probe, (2) the BICI heads may be crossed at different cross sections by different probes, and (3) because each probe is located slightly differently in Z_{GSM}.

The solar wind B_Z (as measured by the WIND spacecraft and shifted to 1 AU; not shown here) on 15 February 2008 between 4:00 and 5:20 UT was almost always positive. Between 5:20 and 11:00 UT the solar wind B_Z has switched many times between positive and negative values. Hence, a continuous compression of the plasma sheet during this period due to permanently enhancing lobe field cannot explain the current sheet stretching and thinning between 4:00 and 6:15 UT. Additionally, a B_Z dip with the radial size of about 2.5 R_E and the azimuthal size that could be as large as 10 R_E was indicated during over 3 hr of observations at $X_{\mathrm{GSM}} \approx -11\ R_E$. Note that previously only scarce direct or some indirect evidence for the presence of magnetic field minima in the transition region between the dipole and tail fields has been reported (Sergeev et al., 2018).

The absence of a permanent loading of the reconnected lobe field and the formation of a thin current sheet within a thicker plasma sheet with a local B_Z dip suggests that a spatial rearrangement of the magnetic flux has occurred. The magnetic flux rearrangement idea is consistent with the magnetic field and pressure observations at P3/P4 and P1 between 5:00 and 6:00 UT. Such a process was predicted to occur in the transition region between the dipole and tail fields (Pritchett & Coroniti, 1994, 1995) as a consequence of the imposition of a dawn to dusk electric field E_y. Note that the total E_y need not be dawnward, while the total convection E_y field is directed duskward and thus drives an earthward $E \times B$ motion of both the ions and electrons, the flux changes depend only on the inductive portion of E_y that oppose the convective field and thus are directed dawnward. This leads to the tailward motion of flux (see Pritchett & Coroniti, 1995, for details). A finite average E_Z directed toward the center of the plasma sheet and serving to confine the ions electrostatically is present in such current sheets and was clearly exhibited by P2 in Figure 5 between about 9:30 and 10:00 UT. Hence, the present THEMIS observations suggest that the B_Z dip may also be formed in the presence of a polarization E_Z, which could not be addressed by magnetohydrodynamic models.

Since between 9:15 and 10:20 UT probe P2 was crossing the $\partial B_Z/\partial X < 0$ region in the tailward direction, one can also estimate $\partial B_Z/\partial X$ from P2 and P3/P4 data to be of the order of -10 nT/R_E. The δE_Y amplitudes observed by P2, sometimes exceeding 15 mV/m, are significantly stronger than the typical $\delta E_Y \sim$1-mV/m amplitudes found for other reported BICI events with duskward propagations of the BICI heads (Panov, Nakamura, et al., 2012; Panov, Sergeev, et al., 2012). However, probes P3 and P4 observed $\delta E_Y \sim$1 mV/m (not shown here), which is consistent with these events. Hence, this difference in the δE_Y amplitudes at P2 and P3/P4 suggests that P2 was located in a different BICI region, for example, at a steeper part of the tailward B_Z gradient. Indeed, the THEMIS probes' configuration in the event under study between 9:15 and 10:20 UT revealed that P3 and P4 observed the earthward tips of the BICI heads near the B_Z minimum, whereas P2 observed them more in the middle and till the tailward ends.

Note that in both the present charged sheet simulations and in the previous neutral sheet runs (e.g., Pritchett & Coroniti, 2010), numerical constraints stipulated larger value for the initial B_Z field as compared to the in situ observations. This might be the reason for disagreements between the simulations and THEMIS observations in the amplitude of δB_X and δE_Y (δB_X was up to 40% of the lobe field in THEMIS observations but did not exceed 5% of the lobe field in the simulations; δE_Y was several times larger than δE_Z in THEMIS observations but was comparable to δE_Z in the simulations).

A further significant plasma sheet reconfiguration between 6:15 and 6:45 UT that included a northward motion and a dipolarization is associated with a structured moderate (200 km/s on average) earthward flow at P3/P4 (Figures 2b and 2i). A closer look at the flows reveals that this activity is pretty similar to P2 observations in Figure 5 (not shown). Hence, around 6:15 UT THEMIS probes have probably observed the onset of the BICI wave activity in the plasma sheet, which as expected followed the B_Z dip formation. Since the heads are expected to propagate many Earth radii azimuthally, such onset of the BICI activity would inevitably lead to returning the magnetic flux back earthward in a wide magnetic local time sector. In situ, this would be seen as a global (structured) dipolarization, in agreement with THEMIS observations between 6:15 and 6:45 UT (see, e.g., the top panel in Figure 9 of Pritchett & Coroniti, 2010).

As some BICI heads may provoke reconnection onset (Pritchett & Coroniti, 2011, 2013), they would exhibit the properties of localized (with the azimuthal scale on the order of the BICI head size) earthward propagating reconnection (dipolarization) fronts (Nakamura et al., 2002; Runov et al., 2009). A number of small dipolarization-front-like structures were indeed observed between 6:30 and 9:50 UT by some of the THEMIS probes (e.g., P4 at 7:20 UT in Figures 2a and 2i). However, none of these has led to a global dipolarization (Baumjohann et al., 1999) of the near-Earth plasma sheet. This fact suggests that the localized dipolarization fronts tend to return the magnetic flux which was taken from the B_Z minimum tailward during charged thin current sheet formation. These results are actually consistent with PIC simulations (Pritchett & Coroniti, 2011) that showed that a global disruption of the thinned current sheet only occurred in a strongly stretched configuration where the equatorial plasma beta $\beta_{eq} = P_p/P_{Bz} \approx 500$. For the case of $\beta_{eq} \leq 100$, no such disruption occurred, consistent with the present observations (Figures 2a and 2h show that P2 at about 6:00 UT and P3/P4 between 6:20 and 6:30 UT indicated the equatorial beta of about 50 with single-point peaks of up to 100).

Although the in situ signatures reported here (the B_Z dip formation, the dawnward wave propagation and the E_Z directed toward the current sheet center) fit well the predictions for the dawnward propagating BICI heads in the PIC simulations for a charged current sheet, further ionospheric-plasma sheet conjugate observations are needed to discuss the possible relation of the BICI heads with various AAFs. Note that most of auroral beads/rays were detected around the substorm onset time, when buoyancy oscillations may cause bidirectional azimuthal propagation of the buoyancy waves between the near-Earth plasma sheet and the plasmapause from a common source (Wolf et al., 2018).

5. Conclusions

THEMIS observations on 15 February 2008 between 04:00 and 11:00 UT in the near-Earth plasma sheet revealed that a B_Z dip with radial size of about 2.5 R_E and azimuthal size that could be as large as 10 R_E persisted for over 3 hr in the plasma sheet at $X_{GSM} \approx -11$ R_E. A finite average E_Z directed toward the center of the plasma sheet, found by THEMIS, is consistent with the idea of a charged diamagnetic thin current sheet formation in the transition region between the dipole and tail fields. In accord with the PIC simulations of the charged current sheet, the dawnward azimuthal propagation of the BICI heads that were observed at the tailward side of the dip with $\partial B_Z/\partial x \approx -10$ nT/R_E is due to change of the cross-tail current carrier direction in the thin current sheet, in which electrons carry all of the cross-tail current.

Acknowledgments
We acknowledge NASA contract NAS5-02099 for use of data from the THEMIS Mission and, specifically, for the use of FGM data supported through the German Ministry for Economy and Technology and the German Center for Aviation and Space (DLR) under contract 50 OC 0302. For the GBO/ASIs, we acknowledge S. Mende and E. Donovan, NASA contract NAS5-02099 and the CSA for logistical support in fielding and data retrieval from the GBO stations. The THEMIS data were obtained freely from Space Sciences Laboratory-University of California, Berkeley (ftp://themis.ssl.berkeley.edu/data/themis/). The work of PLP was supported by NASA grant NNX14AF70G. The particle simulations were made possible by an allocation of advanced computing resources provided by the NASA High-End Computing (HEC) Program through the NASA Advanced Supercomputing (NAS) Division at Ames Research Center. The PIC simulation setup and data can be found in supporting information S1–S5. The work of EVP was partly supported by the Austrian Science Fund (FWF): I 3506-N27. The authors thank Marina Kubyshkina for helpful discussions. This paper initiated from discussions within the framework of the international team "Explosive Processes in the Magnetotail: Reconnection Onset and Associated Plasma Instabilities" supported by the International Space Science Institute (ISSI), including two dedicated workshops held in Bern, Switzerland, in October 2016 and 2017.

References

Angelopoulos, V. (2008). The THEMIS mission. *Space Science Reviews*, *141*, 5–34. https://doi.org/10.1007/s11214-008-9336-1

Auster, H. U., Glassmeier, K. H., Magnes, W., Aydogar, O., Baumjohann, W., Constantinescu, D., et al. (2008). The THEMIS fluxgate magnetometer. *Space Science Reviews*, *141*, 235–264. https://doi.org/10.1007/s11214-008-9365-9

Baumjohann, W., Hesse, M., Kokubun, S., Mukai, T., Nagai, T., & Petrukovich, A. A. (1999). Substorm dipolarization and recovery. *Journal of Geophysical Research*, *104*(24), 24,995–25,000. https://doi.org/10.1029/1999JA900282

Bonnell, J. W., Mozer, F. S., Delory, G. T., Hull, A. J., Ergun, R. E., Cully, C. M., et al. (2008). The Electric Field Instrument (EFI) for THEMIS. *Space Science Reviews*, *141*, 303–341. https://doi.org/10.1007/s11214-008-9469-2

Donovan, E., Mende, S., Jackel, B., Frey, H., Syrjäsuo, M., Voronkov, I., et al. (2006). The THEMIS all-sky imaging array–system design and initial results from the prototype imager. *Journal of Atmospheric and Solar-Terrestrial Physics*, *68*, 1472–1487. https://doi.org/10.1016/j.jastp.2005.03.027

Elphinstone, R. D., Hearn, D. J., Cogger, L. L., Murphree, J. S., Singer, H., Sergeev, V., et al. (1995). Observations in the vicinity of substorm onset: Implications for the substorm process. *Journal of Geophysical Research*, *100*, 7937–7969. https://doi.org/10.1029/94JA02938

Gallardo-Lacourt, B., Nishimura, Y., Lyons, L. R., Ruohoniemi, J. M., Donovan, E., Angelopoulos, V., et al. (2014). Ionospheric flow structures associated with auroral beading at substorm auroral onset. *Journal of Geophysical Research: Space Physics*, *119*, 9150–9159. https://doi.org/10.1002/2014JA020298

Hau, L.-N. (1991). Effects of steady state adiabatic convection on the configuration of the near-Earth plasma sheet. II. *Journal of Geophysical Research*, *96*, 5591–5596. https://doi.org/10.1029/90JA02619

Hau, L.-N., Wolf, R. A., Voigt, G.-H., & Wu, C. C. (1989). Steady state magnetic field configurations for the Earth's magnetotail. *Journal of Geophysical Research*, *94*, 1303–1316. https://doi.org/10.1029/JA094iA02p01303

Hsieh, M.-S., & Otto, A. (2015). Thin current sheet formation in response to the loading and the depletion of magnetic flux during the substorm growth phase. *Journal of Geophysical Research: Space Physics*, *120*, 4264–4278. https://doi.org/10.1002/2014JA020925

Kalmoni, N. M. E., Rae, I. J., Watt, C. E. J., Murphy, K. R., Forsyth, C., & Owen, C. J. (2015). Statistical characterization of the growth and spatial scales of the substorm onset arc. *Journal of Geophysical Research: Space Physics*, *120*, 8503–8516. https://doi.org/10.1002/2015JA021470

Liang, J., Donovan, E. F., Liu, W. W., Jackel, B., Syrjäsuo, M., Mende, S. B., et al. (2008). Intensification of preexisting auroral arc at substorm expansion phase onset: Wave-like disruption during the first tens of seconds. *Geophysical Research Letters*, *35*, L17S19. https://doi.org/10.1029/2008GL033666

McFadden, J. P., Carlson, C. W., Larson, D., Ludlam, M., Abiad, R., Elliott, B., et al. (2008). The THEMIS ESA plasma instrument and in-flight calibration. *Space Science Reviews*, *141*, 277–302. https://doi.org/10.1007/s11214-008-9440-2

Motoba, T., Hosokawa, K., Kadokura, A., & Sato, N. (2012). Magnetic conjugacy of northern and southern auroral beads. *Geophysical Research Letters*, *39*, L08108. https://doi.org/10.1029/2012GL051599

Motoba, T., Hosokawa, K., Ogawa, Y., Sato, N., Kadokura, A., Milan, S. E., & Lester, M. (2012). Simultaneous ground-satellite observations of meso-scale auroral arc undulations. *Journal of Geophysical Research*, *117*, A06213. https://doi.org/10.1029/2011JA017291

Nakamura, R., Baumjohann, W., Klecker, B., Bogdanova, Y., Balogh, A., Rème, H., et al. (2002). Motion of the dipolarization front during a flow burst event observed by Cluster. *Geophysical Research Letters*, *29*(20), 1942. https://doi.org/10.1029/2002GL015763

Nishimura, Y., Lyons, L. R., Nicolls, M. J., Hampton, D. L., Michell, R. G., Samara, M., et al. (2014). Coordinated ionospheric observations indicating coupling between preonset flow bursts and waves that lead to substorm onset. *Journal of Geophysical Research: Space Physics*, *119*, 3333–3344. https://doi.org/10.1002/2014JA019773

Nishimura, Y., Yang, J., Pritchett, P. L., Coroniti, F. V., Donovan, E. F., Lyons, L. R., et al. (2016). Statistical properties of substorm auroral onset beads/rays. *Journal of Geophysical Research: Space Physics*, *121*, 8661–8676. https://doi.org/10.1002/2016JA022801

Panov, E. V., Nakamura, R., Baumjohann, W., Kubyshkina, M., Artemyev, A., Sergeev, V. A., et al. (2012). Kinetic ballooning/interchange instability in a bent plasma sheet. *Journal of Geophysical Research*, *117*, A06228. https://doi.org/10.1029/2011JA017496

Panov, E. V., Sergeev, V. A., Pritchett, P. L., Coroniti, F. V., Nakamura, R., Baumjohann, W., et al. (2012). Observations of kinetic ballooning/interchange instability signatures in the magnetotail. *Geophysical Research Letters*, *39*, L08110. https://doi.org/10.1029/2012GL051668

Pritchett, P. L., & Coroniti, F. V. (1994). Convection and the formation of thin current sheets in the near-Earth plasma sheet. *Geophysical Research Letters*, *21*, 1587–1590. https://doi.org/10.1029/94GL01364

Pritchett, P. L., & Coroniti, F. V. (1995). Formation of thin current sheets during plasma sheet convection. *Journal of Geophysical Research*, *100*, 23,551–23,566. https://doi.org/10.1029/95JA02540

Pritchett, P. L., & Coroniti, F. V. (2010). A kinetic ballooning/interchange instability in the magnetotail. *Journal of Geophysical Research*, *115*, A06301. https://doi.org/10.1029/2009JA014752

Pritchett, P. L., & Coroniti, F. V. (2011). Plasma sheet disruption by interchange-generated flow intrusions. *Geophysical Research Letters*, *38*, L10102. https://doi.org/10.1029/2011GL047527

Pritchett, P. L., & Coroniti, F. V. (2013). Structure and consequences of the kinetic ballooning/interchange instability in the magnetotail. *Journal of Geophysical Research: Space Physics*, *118*, 146–159. https://doi.org/10.1029/2012JA018143

Pritchett, P. L., Coroniti, F. V., & Nishimura, Y. (2014). The kinetic ballooning/interchange instability as a source of dipolarization fronts and auroral streamers. *Journal of Geophysical Research: Space Physics*, *119*, 4723–4739. https://doi.org/10.1002/2014JA019890

Rae, I. J., Watt, C. E. J., Mann, I. R., Murphy, K. R., Samson, J. C., Kabin, K., & Angelopoulos, V. (2010). Optical characterization of the growth and spatial structure of a substorm onset arc. *Journal of Geophysical Research*, *115*, A10222. https://doi.org/10.1029/2010JA015376

Runov, A., Angelopoulos, V., Sitnov, M. I., Sergeev, V. A., Bonnell, J., McFadden, J. P., et al. (2009). THEMIS observations of an earthward-propagating dipolarization front. *Geophysical Research Letters*, *36*, L14106. https://doi.org/10.1029/2009GL038980

Saito, M. H., Hau, L.-N., Hung, C.-C., Lai, Y.-T., & Chou, Y.-C. (2010). Spatial profile of magnetic field in the near-Earth plasma sheet prior to dipolarization by THEMIS: Feature of minimum B. *Geophysical Research Letters*, *37*, L08106. https://doi.org/10.1029/2010GL042813

Sakaguchi, K., Shiokawa, K., & Donovan, E. (2009). Azimuthal structures of ray auroras at the beginning of auroral substorms. *Geophysical Research Letters*, *36*, L23106. https://doi.org/10.1029/2009GL041252

Sergeev, V. A., Gordeev, E. I., Merkin, V. G., & Sitnov, M. I. (2018). Does a local B-minimum appear in the tail current sheet during a substorm growth phase? *Geophysical Research Letters*, *45*, 2566–2573. https://doi.org/10.1002/2018GL077183

Sitnov, M. I., Merkin, V. G., Swisdak, M., Motoba, T., Buzulukova, N., Moore, T. E., et al. (2014). Magnetic reconnection, buoyancy, and flapping motions in magnetotail explosions. *Journal of Geophysical Research: Space Physics*, *119*, 7151–7168. https://doi.org/10.1002/2014JA020205

Tang, C.-L. (2011). The wave-like auroral structure around auroral expansion onset. *Chinese Physics Letters*, *28*(10), 109401. https://doi.org/10.1088/0256-307X/28/10/109401

Uritsky, V. M., Liang, J., Donovan, E., Spanswick, E., Knudsen, D., Liu, W., et al. (2009). Longitudinally propagating arc wave in the pre-onset optical aurora. *Geophysical Research Letters*, *36*, L21103. https://doi.org/10.1029/2009GL040777

Wolf, R. A., Toffoletto, F. R., Schutza, A. M., & Yang, J. (2018). Buoyancy waves in Earth's magnetosphere: Calculations for a 2D wedge magnetosphere. *Journal of Geophysical Research: Space Physics*, *123*, 3548–3564. https://doi.org/10.1029/2017JA025006